THE ASTROPHYSICAL JOURNAL, 350:437–451, 1990 February 10

THE LINEAR STABILITY OF LINE-TIED CORONAL MAGNETIC FIELDS

B. J. FOOTE AND I. J. D. CRAIG
Department of Mathematics, University of Waikato, Hamilton, New Zealand
Received 1988 November 18; accepted 1989 October 5

ABSTRACT

The problem of the linear stability of cylindrically symmetric force-free magnetic equilibria is addressed. The aim is to quantify the severity of ideal MHD disturbances on a variety of line-tied coronal equilibria. Accordingly methods are developed which determine, at high spatial resolution, the dominant eigenmodes of the problem.

We first introduce a family of equilibrium force-free fields parameterized by the local dimensionless twist $T = r^{\nu}$ which includes the well-known Gold-Hoyle field in the case $\nu = 0$. The stability problem is then formulated, and the numerical techniques required for its solution are derived. As a preliminary test of our methods we present convergence results for the critical length of the Gold-Hoyle field, obtaining the result $l_c = 2.46\pi$ (dimensionless units).

Next, the severity of the instability is quantified. The kink instability ($m = 1$) is found to be weak even for long lengths ($l \gtrsim 4l_c$), generating dimensionless force eigenvalues less than $O(10^{-2})$. The Gold-Hoyle field is shown to be the most unstable member of the family for large l, yet is the most susceptible to line-tying and so possesses the longest critical length. Preliminary investigations for higher m have not yielded instabilities for the moderate tube lengths of interest.

The significance of these results to flare theories cannot be known definitively without results from finite-amplitude studies. Our results show, however, that the power release over the linear phase is at least *three orders of magnitude* below dimensional expectation. This implies that unstable coronal flux tubes cannot be expected to collapse violently on the MHD time scale.

Subject headings: hydromagnetics — instabilities — Sun: corona — Sun: flares

I. INTRODUCTION

Solar flares are generally believed to be caused by the rapid (of order 100 s) collapse of magnetic fields in the solar corona (e.g., Švestka 1976). Much effort has gone into theoretical flare studies, and it appears that a promising candidate for triggering the rapid release of magnetic energy is the ideal MHD instability, in particular the corkscrew kink associated with twisted magnetic flux tubes. All infinitely long cylindrical flux tubes are kink-unstable (Anzer 1968), but when the effects of "line-tying" at the ends of a finite loop are taken into account, the loop may be stabilized if sufficiently short, as first demonstrated by Raadu (1972) and refined by later workers (Hood and Priest 1981; Einaudi and Van Hoven 1983). This implies that a flux tube, which is slowly being twisted up by photospheric motions of the footpoints, might suddenly become kink-unstable, and so dramatically release magnetic energy over the explosive flare time scale of typically 100 s.

This theoretical picture, however, is clouded by the remarkable longevity of observed coronal plasma-field configurations: long, thin coronal loops often seem conspicuously quiescent in apparent violation of the rather stringent theoretical "line-tied" stability condition (see § IV*b*). In addition, Craig, McClymont, and Sneyd (1988) have demonstrated—at least for Gold-Hoyle equilibria—that the corkscrew kink is remarkably feeble, generating Lorentz forces two or more orders of magnitude below dimensional expectation. This agrees with the infinite tube results of Sneyd and Craig (1989), while Goedbloed and Hagebeuk (1972) have demonstrated weak instabilities for the infinite Lundquist field. These results impact not only on linear growth times, although these are increased by at least an order of magnitude, but more critically on the *power released* during the linear phase of the instability which suffers a devastating reduction of 1000-fold or greater. The full implications of these results are not yet clear, but there is an obvious need to analyze more general magnetic field equilibria and to extend the linear analysis into the nonlinear regime.

In this paper we tackle the first of these objectives by quantifying the linear stability of line-tied, cylindrical flux tubes under the assumption of an ignorable azimuthal coordinate for the equilibrium field. This simplification means that the eigenmodes of the problem possess an $e^{im\theta}$ dependence and leads to an effective reduction in the space dimensionality of the problem. Our study therefore complements Craig, McClymont, and Sneyd (1988), who develop general methods for determining the eigenmodes of arbitrary magnetic fields in the absence of spatial symmetries, and Sneyd and Craig (1989), who calculate eigenmodes for infinitely long flux tubes. Our analysis also refines and generalizes the results of Hood and Priest (1981) and Einaudi and Van Hoven (1983), who estimate the critical length of the line-tied Gold-Hoyle field but who do not quantify the magnitude of the instability. In turn, our analysis is complemented by finite-amplitude studies (Craig and Sneyd 1986) of the corkscrew kink disturbance.

In § II we give the background of the linear stability problem and introduce a one-parameter family of force-free flux tubes which are nonuniformly twisted but incorporate the well-known Gold-Hoyle field as a special case. Section III develops the analytic and computational machinery required for determining the eigensystem of the force operator: our basic techniques are the power and inverse power methods discussed by Craig, McClymont, and Sneyd (1988) but fine-tuned for the problem in hand. In § IV we quantify the instability by determining the dominant force eigenvalues and the critical (i.e., marginally stable) length of the

equilibrium field. The implications of these results to quiescent and active solar plasmas are discussed in § V, while § VI lists our conclusions.

II. LOOP EQUILIBRIUM AND ITS LINEAR STABILITY

a) *Basic Assumptions*

Observation shows coronal loops to be structures with low toroidal nature, so it seems reasonable to neglect toroidal effects entirely and to model a coronal loop by a straight flux tube with ends at $z = 0, l$ where it meets the photosphere. Observation further indicates high axial uniformity in loops, so with the added assumption of cylindrical symmetry, the flux tube has the structure (cylindrical polars):

$$\boldsymbol{B} = [0,\ B_\theta(r),\ B_z(r)]\ . \tag{2.1}$$

In general this describes a twisted flux tube, where any given field line wraps around a cylindrical surface with a twist

$$T(r) = \frac{B_\theta(r)}{rB_z(r)}\ , \tag{2.2}$$

meaning that the total twist of a field line in passing from one end of the tube to the other is simply $lT(r)$.

In what follows it is assumed that coronal fluid experiences a Lorentz force only. Thus, the influence of plasma pressure both on the perturbed and unperturbed system is assumed to be negligible. Forces due to fluid viscosity and gravity are also neglected. Together with the assumption of constant-density corona, we arrive at a simple model of a coronal loop, but nevertheless one which is amenable to analysis and still contains all the essential physics.

b) *Equilibrium Field*

Under the previous assumptions, the equilibrium flux tube must be *force-free;* i.e., it must satisfy

$$\frac{d}{dr}\left(\frac{1}{2}\,B^2\right) + \frac{B_\theta^2}{r} = 0\ , \tag{2.3}$$

an expression of balance between magnetic tension and gradients in magnetic pressure. Note that equation (2.3) lacks completeness in the sense that the one equation contains two unknowns, so information must be supplied to permit its unique solution. If we specify the twist $T(r)$, we find (Sneyd and Craig 1989)

$$\frac{B_z}{B_z(0)} = \frac{1}{1 + r^2T^2}\exp\left(\int_0^r \frac{r^2TT'}{1 + r^2T^2}\,dr\right),$$
$$B_\theta = rTB_z\ . \tag{2.4}$$

In this paper we study a simple family of solutions with the power-law twist

$$aT = \left(\frac{r}{a}\right)^\nu, \qquad \frac{B_z}{B_0} = \left[1 + \left(\frac{r}{a}\right)^{2(1+\nu)}\right]^{-(1+\nu/2)/(1+\nu)}, \tag{2.5}$$

where a, the "tube radius," is a radial length scale. We assume $\nu \geq 0$ to avoid a current singularity at the origin. In the special case $\nu = 0$, we recover the much-studied uniform-twist field of Gold and Hoyle, which corresponds to a rigid-body rotation of the photospheric "endplates." As ν increases, the currents become increasingly concentrated about the shell $r = a$, approaching as $\nu \to \infty$ the "idealized field" studied by previous workers (Kruskal and Tuck 1958; Hood and Priest 1981), namely:

$$\frac{\boldsymbol{B}}{B_0} = \begin{cases} (0,\ 0,\ 1) & \text{for } r/a < 1\ , \\ (0,\ a/r,\ 0) & \text{for } r/a > 1\ , \end{cases} \tag{2.6}$$

with the current density profile $\boldsymbol{j} = (B_0/4\pi r)\delta(r - a)(\hat{\boldsymbol{\theta}} + \hat{\boldsymbol{z}})$. Graphs of the magnetic field components for various ν are presented in Figure 1.

c) *Stability Equations*

The ideal MHD stability of the force-free flux tube is now examined by considering the effect of a small fluid displacement $\boldsymbol{\xi}(\boldsymbol{x}, t)$. The resulting magnetic field perturbation is found by time integration (to first order) of the induction equation to be

$$\delta\boldsymbol{B} = \nabla \times (\boldsymbol{\xi} \times \boldsymbol{B})\ , \tag{2.7}$$

and so the Lorentz force is, to first order in perturbed quantities,

$$\boldsymbol{F}(\xi) = \frac{1}{4\pi}\left[(\nabla \times \delta\boldsymbol{B}) \times \boldsymbol{B} + (\nabla \times \boldsymbol{B}) \times \delta\boldsymbol{B}\right]\ . \tag{2.8}$$

Displacements then evolve according to the equation of motion

$$\rho\,\frac{\partial^2\boldsymbol{\xi}}{\partial t^2} = \boldsymbol{F}(\xi)\ . \tag{2.9}$$

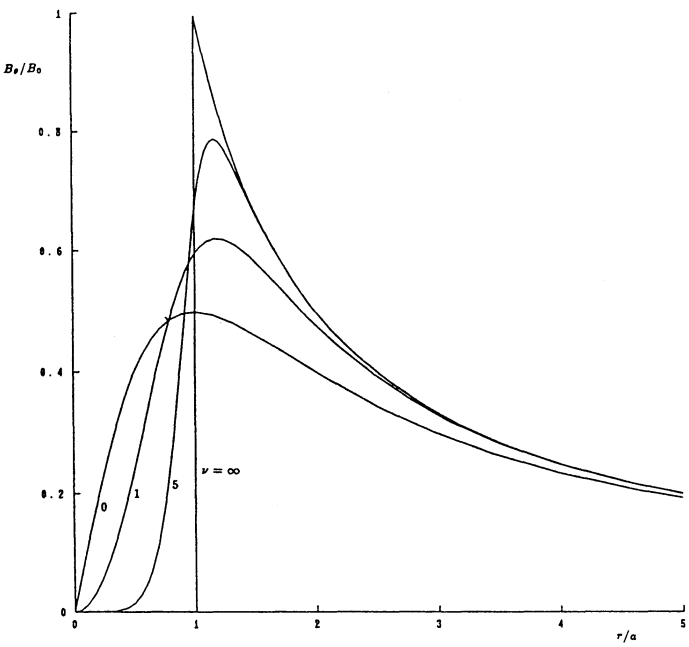

FIG. 1a

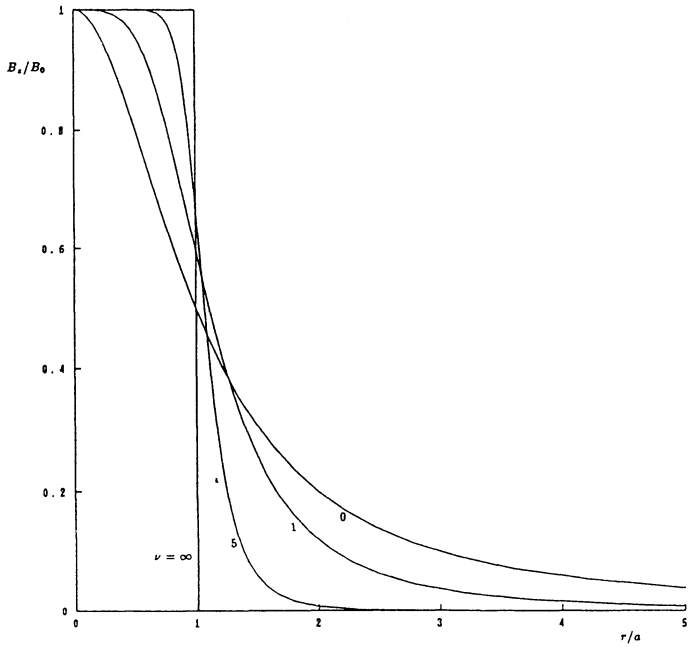

FIG. 1b

FIG. 1.—Components (*a*) $B_\theta(r)$ and (*b*) $B_z(r)$ for a flux tube with twist $aT = (r/a)^\nu$ (see eq. [2.5]), for $\nu = 0$, 1, 5, and ∞.

Introducing the nondimensional variables,

$$r' = r/a\,, \qquad \xi' = \xi/a\,, \qquad \boldsymbol{B}' = \boldsymbol{B}/B_0\,, \qquad t' = tv_A/a\,, \tag{2.10}$$

where a, B_0 are characteristic values of length and magnetic field strength, respectively, and $v_A = B_0/(4\pi\rho)^{1/2}$ is a characteristic Alfvén speed, this equation becomes (dropping dashes)

$$\frac{\partial^2 \boldsymbol{\xi}}{\partial t^2} = \boldsymbol{F}(\boldsymbol{\xi}) = (\nabla \times \delta\boldsymbol{B}) \times \boldsymbol{B} + (\nabla \times \boldsymbol{B}) \times \delta\boldsymbol{B}\,. \tag{2.11}$$

The symmetry of the equilibrium field implies that eigendisplacements possess the normal mode form

$$\boldsymbol{\xi}(r, \theta, z, t) = \boldsymbol{\xi}(r, z)e^{i(m\theta + \omega t)}\,, \tag{2.12}$$

where $m = 0, 1, 2, \ldots$, and ω is a complex frequency. Such an eigendisplacement obeys

$$\lambda\boldsymbol{\xi} = \boldsymbol{F}(\boldsymbol{\xi})\,, \tag{2.13}$$

where $\lambda = -\omega^2$. Thus $\boldsymbol{\xi}$ is an eigenfunction of the force operator $\boldsymbol{F}$. Bernstein *et al.* (1958) have shown $\boldsymbol{F}$ to be self-adjoint; i.e., for all $\boldsymbol{\xi}, \boldsymbol{\eta}$ satisfying the appropriate boundary conditions:

$$\langle \boldsymbol{F}(\boldsymbol{\xi}), \boldsymbol{\eta} \rangle = \langle \boldsymbol{\xi}, \boldsymbol{F}(\boldsymbol{\eta}) \rangle\,, \tag{2.14}$$

where the inner product is defined by

$$\langle \boldsymbol{\xi}, \boldsymbol{\eta} \rangle = \int_V d\tau \boldsymbol{\xi} \cdot \bar{\boldsymbol{\eta}}\,. \tag{2.15}$$

Accordingly, we have a real eigenvalue spectrum $\lambda_1 \geq \lambda_2 \geq \lambda_3 \ldots$.

Since pressure effects are neglected, and, to first order, the Lorentz force is perpendicular to the equilibrium field $\boldsymbol{B}$, then so is any eigendisplacement (see eq. [2.13]). It follows that an entirely general form for $\boldsymbol{\xi}$ is (Sneyd and Craig 1990)

$$\boldsymbol{\xi}(r, z) = \left[\frac{P(r, z)}{B_z}, B_z \frac{Q(r, z)}{B^2}, -rTB_z \frac{Q(r, z)}{B^2}\right], \tag{2.16}$$

where $P(r, z)$, $Q(r, z)$ are complex functions. By choosing $\boldsymbol{\xi}$ in this manner we have simplified the form of

$$\boldsymbol{\xi} \times \boldsymbol{B} = (Q, -P, rTP)\,; \tag{2.17}$$

furthermore since according to the force-free condition we may write

$$\nabla \times \boldsymbol{B} = \alpha(r)\boldsymbol{B}\,, \qquad \alpha = \frac{rT' + 2T}{1 + r^2T^2}\,, \tag{2.18}$$

it follows that the eigenvalue equation contains B_z as a multiplicative factor only. The respective θ- and r-components are found to be

$$\lambda \frac{Q}{B^2} = \alpha\left(\frac{\partial}{\partial z} + imT\right)P + \frac{im}{r^2}\frac{\partial}{\partial r}(rP) - \frac{\partial}{\partial r}\left(rT\frac{\partial P}{\partial z}\right) + \frac{\partial^2 Q}{\partial z^2} - \frac{m^2}{r^2}Q ,$$

$$\frac{1}{B_z}\lambda\frac{P}{B_z} = \left(\frac{\partial}{\partial z} + imT\right)^2 P + \alpha r T' P + \frac{\partial}{\partial r}\left[\frac{1}{r}\frac{\partial}{\partial r}(rP)\right] + T\frac{\partial}{\partial r}\left[r\frac{\partial}{\partial r}(rTP)\right]$$

$$+ im\frac{\partial}{\partial r}\left(\frac{Q}{r}\right) - T\frac{\partial}{\partial r}\left(r\frac{\partial Q}{\partial z}\right) - \alpha\left(\frac{\partial}{\partial z} + imT\right)Q , \tag{2.19}$$

the z-component yielding an expression identical to the θ-component. Our aim is to solve these equations for given m, subject to the boundary conditions developed below. Because of their complexity, the equations must in general be solved numerically. Methods for performing this are described in § III.

d) Boundary Conditions

As first discussed by Raadu (1972), a realistic loop model must take account of the rooting of field lines in the dense photosphere at each end of the loop. A simplifying idealization of this phenomenon is that of *line-tying*, whereby fluid displacement *vanishes* at the ends:

$$P(r, z), Q(r, z) = 0 \quad \text{at} \quad z = 0, l . \tag{2.20}$$

Ideally, we would assume the fluid displacement to vanish at $r = \infty$:

$$\frac{P}{B_z}, \frac{B_z Q}{B^2} \to 0 \quad \text{as} \quad r \to \infty . \tag{2.21}$$

Computationally, however, we imagine that displacements vanish at a finite radius b,

$$P(b, z) = Q(b, z) = 0 . \tag{2.22}$$

Provided the outer boundary is placed far beyond the region of intense magnetic field, we expect this to have little practical consequence. Strictly, the conditions (2.22) are inconsistent with the placement of a perfectly conducting cylinder at $r = b$ since in this case we cannot necessarily impose $Q(b, z) = 0$. However, once again provided $b \gg 1$, imposing this extra condition has little effect on unstable modes—the ones of prime physical interest.

As discussed in Appendix A, the conditions on the axis are found by demanding finiteness of the physical quantities $\nabla\boldsymbol{\xi}$, $\boldsymbol{j}$ the current density, and $\boldsymbol{F}(\boldsymbol{\xi})$ the Lorentz force to be

$$\begin{aligned} P_r(0, z) = Q_r(0, z) = 0 \qquad & \text{if } m = 1 , \\ P(0, z) = \ Q(0, z) = 0 \qquad & \text{if } m \neq 1 . \end{aligned} \tag{2.23}$$

The same conditions are derived by Hood and Priest (1981), but in less generality since they restrict the equilibrium B_z to a power series in r^2. In fact, we need only assume T finite and smooth as $r \to 0$, so that $\boldsymbol{j}$ is correspondingly nonsingular (see eq. [2.18]). We note the first of the fields studied numerically by Anzer (1968) does not satisfy this physical requirement!

e) Physical Significance of the Force Eigenvalues

The force eigenvalues contain the totality of information on the growth or decay time of an instability in its linear phase and on the magnitude of energy release. Specifically, an eigendisplacement $\boldsymbol{\xi}$ with corresponding eigenvalue λ evolves as $\exp[t(\lambda)^{1/2}]$, so its growth time is $\lambda^{-1/2}$ (units $t_A = a/v_A$). Thus, the eigendisplacement becomes more unstable as λ increases, the transition from stability to instability occurring at $\lambda = 0$. Also the energy density of a fluid element is given by

$$M(\boldsymbol{x}, t) = \tfrac{1}{2}\boldsymbol{F}(\boldsymbol{\xi}) \cdot \boldsymbol{\xi} = \tfrac{1}{2}\lambda|\boldsymbol{\xi}|^2 , \tag{2.24}$$

so the power density is

$$P(\boldsymbol{x}, t) = \frac{\partial M}{\partial t} = \lambda^{3/2}|\boldsymbol{\xi}|^2 . \tag{2.25}$$

Thus, it is seen that the power of an instability has a dramatic cubic dependence on the growth rate.

Of course, the growth rate of the field is that of the most unstable eigenmode (over all m). All axisymmetric $m = 0$ modes are stable for an infinite tube (Anzer 1968) and clearly remain so under the stabilizing influence of line-tying. Thus, in what follows, we consider only $m = 1$ modes or higher. For an infinite tube, the $m = 1$ helical kink mode is suspected to give the strongest instabilities, a suspicion confirmed for the Gold-Hoyle field in particular (Sneyd and Craig 1989). However, since all previous work has considered *only* $m = 1$, it is uncertain whether this obtains for the line-tied tube.

III. DETERMINATION OF THE EIGENSYSTEM OF THE FORCE OPERATOR

a) Introduction

Our approach to the problem is based on the idea of integrating the dimensionless "fictitious" force equation

$$\dot{\boldsymbol{\xi}} = \boldsymbol{F}(\boldsymbol{\xi}) \tag{3.1}$$

forward in time. Given an arbitrary initial displacement, the system is allowed to evolve until the least stable mode predominates: in this way the dominant mode is isolated, irrespective of whether it grows or decays in time. If we assume *a priori* the existence of the normal mode decomposition, then the method fails only in the pathological case where the initial disturbance contains no component of the dominant physical mode. If no normal modes exist, then the time-integration procedure will fail to isolate a solution that varies in amplitude but retains its spatial form.

The idealized dimensionless formulation we adopt, in which gas pressure effects are neglected, leads to three major simplifications. First, the eigenvalues of the force operator $\boldsymbol{F}$ are pure numbers which are uncompromised by extraneous parameters describing the background plasma distribution and depend only on the azimuthal mode number m and the length (in units a) of the line-tied field. Thus, once the equilibrium field is specified, there are no free parameters in the analysis. Of course, to interpret force eigenvalues *a posteriori* in terms of actual growth rates we need to assume a value for the (constant) density of the background coronal plasma. Second, plasma perturbations are determined entirely by the field and may be arbitrarily compressible—although we would expect the least stable mode to be close to incompressible near marginal stability (see, for example, Van Hoven 1981). Third, the eigenvalue problem is reduced to determining just two independent components of the displacement, as mentioned in § II*c*.

In what follows we choose the representation (denoted by light-faced characters)

$$\xi = \begin{pmatrix} P \\ Q \end{pmatrix}. \tag{3.2}$$

Thus, according to equation (2.19), ξ evolves as $\dot{\xi} = \lambda\xi = F(\xi)$. Here F is the operator in our chosen representation. Of course, the *physical* eigendisplacements $\boldsymbol{\xi}$ are determined via equation (2.16).

b) Spatial Discretization

To obtain explicit eigensolutions the evolution equation must be implemented in computational form. Our basic numerical techniques are the cyclic power and inverse power methods, as discussed by Craig, McClymont, and Sneyd (1988).

First, the problem is discretized: we represent the rz-plane by the mesh $r = r_j$, $z = z_k$ for $j = 0, 1, \ldots, n_r$ and $k = 0, 1, \ldots, n_z$. We wish the mesh to be nonuniform in the r-direction to allow b large while still maintaining resolution within the "tube radius." Thus, we choose to formulate the problem in an $\eta\zeta$-plane, related to the rz-plane by the transformation $r = r(\eta)$, $z = z_\zeta \zeta$, with a uniform $\eta\zeta$-mesh:

$$\eta_j = j\Delta\,, \qquad \zeta_k = k\Delta\,, \qquad \Delta = \frac{1}{n_r} \qquad \text{for } j = 0, 1, \ldots, n_r\,, \qquad k = 0, 1, \ldots, n_z\,. \tag{3.3}$$

Points are distributed over $0 \le \eta \le 1$, $0 \le \zeta \le n_z/n_r$, so that by varying l and n_z in proportion the mesh resolution is left roughly unchanged. A transformation commonly used in this paper is

$$r = b\eta\,\frac{1 - c^2}{1 - c^2\eta^2}\,, \tag{3.4}$$

which becomes increasingly nonlinear as c^2 increases from zero. Typically, c^2 is chosen so that the *half-radius* $r_{1/2} \equiv r(\eta = \frac{1}{2})$, inside which half the points lie, is of order the "tube radius" $r = 1$.

Under spatial discretization, exact eigenfunctions become replaced by numerical representations defined at the mesh nodes only. Oscillation on a scale less than the mesh spacing Δ can no longer be represented. This results in the truncation of the eigenvalue spectrum: $\lambda_1, \lambda_2, \ldots, \lambda_M$, where the *mesh mode* (λ_M, ξ_M) represents a strongly stable eigenfunction oscillating on the mesh wavelength.

c) Solution via Power and Inverse Power Iterations

i) Introduction

The power iteration is ideally suited to the solution of the system (2.13). Explicit storage of the operator F (in our discrete representation) is bypassed, and convergence can be made automatic to the dominant mode, the one of prime physical interest. In the standard power method, iteration proceeds according to

$$\xi^{(n+1)} = (F + \Lambda I)\xi^{(n)}\,, \tag{3.5}$$

which can be viewed as an explicit time-integration scheme with the *shift parameter* Λ playing the role of an inverse time step, as discussed by Craig, McClymont, and Sneyd (1988). As shown in Wilkinson (1965), the choice of $\Lambda = \Lambda_{\rm opt} \equiv -\frac{1}{2}(\lambda_2 + \lambda_M)$ gives the best convergence rate of

$$c_{\rm opt} = 1 - \frac{\lambda_1 - \lambda_2}{\lambda_1 + \Lambda_{\rm opt}}\,. \tag{3.6}$$

Now in practice the dominant eigenvalues are weak and $|\lambda_M| \gg |\lambda_1|$, meaning that convergence can be very slow, worsening as the spatial resolution increases. This problem can be overcome by the introduction of *cyclic* shifts, as detailed in § IIIc(ii).

An alternative stratagem is to invoke the inverse power iteration, defined by

$$(F + \Lambda' I)\xi^{(n+1)} = \xi^{(n)} . \tag{3.7}$$

This scheme potentially provides a highly effective technique for computing the eigensystem, but has the disadvantage of requiring the storage and decomposition of the discrete operator matrix. In particular, the complex linear system defined by equation (3.7) is resolved using a compact elimination technique (with partial pivoting) to obtain the successive iterates. The iteration converges to the mode whose eigenvalue is closest to Λ', a fixed parameter specified by the user. The iteration is analogous to an unconditionally stable time-integration routine and allows very rapid convergence (often just a few iterations), since it bypasses altogether the restrictions imposed on explicit methods by the large mesh mode. In practice, we find the inverse power method to be the fastest for low-resolution runs, but at higher resolution the power method with cyclic shifts, as discussed below, is superior.

ii) *Acceleration of the Power Method by Cyclic Shifts*

The following discussion refines the development of Craig and Sneyd (1989). Under cyclic variations of the shift parameter Λ, iteration proceeds according to

$$\xi^{(n+1)} = \left[\prod_{l=1}^{N} (F + \Lambda_l I)\right]\xi^{(n)} , \tag{3.8}$$

so that the amplification factor of a mode is now a general polynomial in λ. Writing $x = (\lambda + \Lambda_{\rm opt})/h$, $h = \frac{1}{2}(\lambda_2 - \lambda_M)$ so that all subdominant modes are contained in the interval $[-1, +1]$, we set the amplification factor proportional to $T_N(x)$, the Chebyshev polynomial of order N. This has the desirable property of maximizing the relative amplification of the dominant mode. The effective convergence rate per iteration (of which there are N per cycle) is now

$$c_N(x_1) \equiv \left[\frac{\max\{|T_N(x_l)| : l \neq 1\}}{|T_N(x_1)|}\right]^{1/N} = \frac{1}{[T_N(x_1)]^{1/N}} , \tag{3.9}$$

as $|T_N(x_l)| \leq 1$ for all suppressed modes, with equality for $l = 2$, N in particular. The *best possible* convergence rate occurs in the limit of an infinite cycle:

$$\lim_{N\to\infty} c_N(x_1) = \exp(-\cosh^{-1} x_1) = \frac{1}{x_1 + \sqrt{x_1^2 - 1}} , \tag{3.10}$$

where we have used the fact that $T_N(x) \to \frac{1}{2}\exp(N \cosh^{-1} x)$ as $N \to \infty$. The convergence rate (eq. [3.9]) can be a significant improvement upon the noncyclic one, particularly in the case $x_1 - 1 \ll 1$, the regime of interest, where the power method is least effective. To appreciate the improvement fully, we introduce the *gain factor* $g_N(x_1)$, defined as the number of optimal unshifted iterations compared to the number of iterations using a cycle of length N to attain a specified accuracy. Since, according to equation (3.9), the number of iterations $m_N(x_1, \epsilon)$ required to reduce the error to a level ϵ (assumed much less than the initial error) is $m_N(x_1, \epsilon) \simeq -N \ln \epsilon / \ln T_N(x_1)$, the gain factor is simply

$$g_N(x_1) \equiv \frac{m_1(x_1, \epsilon)}{m_N(x_1, \epsilon)} = \frac{\ln T_N(x_1)}{N \ln x_1} . \tag{3.11}$$

The gain improves as N increases, having the limiting value

$$g_\infty(x_1) \equiv \lim_{N\to\infty} g_N(x_1) = \frac{\ln(x_1 + \sqrt{x_1^2 - 1})}{\ln x_1} . \tag{3.12}$$

For large x_1, the use of cyclic shifts results in little gain. In the other extreme of $\delta \equiv x_1 - 1 \ll 1$, we have $g_\infty(x_1) \sim (2/\delta)^{1/2}$, leading to significant gains. In practice, however, error in the computation of the Chebyshev zeros upsets convergence beyond $N \approx 40$. This means that for a typical value of $\delta = 10^{-5}$ we can achieve a gain of at most 40 or so, less than 1/10 of g_∞, but still very significant.

In practice λ_M, λ_2 will not be known exactly and must be estimated, meaning that the interval over which modes are suppressed differs from $[\lambda_M, \lambda_2]$. Since convergence to the mesh mode can be made rapid, λ_M is readily estimated, and typically we underestimate (ensuring convergence to the dominant mode) by less than 1%. However, λ_2 is difficult to estimate, and so, for want of a better stratagem, it is often set to zero when calculating instabilities. Of course, gains are reduced when such inaccuracies are present (refer to Craig and Sneyd 1989 for details).

We may further accelerate the power method by exploiting the self-adjoint property of the force operator $\boldsymbol{F}$. We estimate the dominant eigenvalue after the nth cycle by the Rayleigh quotient

$$\alpha_N(\lambda_1^{(n+1)}) = \frac{\langle \xi^{(n+1)}, \xi^{(n)} \rangle}{\langle \xi^{(n)}, \xi^{(n)} \rangle} , \tag{3.13}$$

where the volume integral as in equation (2.15) is mimicked using numerical quadrature. Neglecting discretization, the error in this process is quadratic when the operator is self-adjoint (see Isaacson and Keller 1966 for details).

d) Matrix Representation of Operator

We require an explicit matrix representation of the operator F when implementing the inverse power method. This representation is also required in an alternative method, detailed in § III*e*, used for calculations close to marginal stability when the power method becomes relatively slower.

We commence by writing the numerical approximations of $P(\eta_j, \zeta_k)$, $Q(\eta_j, \zeta_k)$ by P_j^k, Q_j^k, respectively, and define the column matrices

$$P_j = \begin{pmatrix} P_j^1 \\ P_j^2 \\ \vdots \\ P_j^{n_z-1} \end{pmatrix}, \qquad Q_j = \begin{pmatrix} Q_j^1 \\ Q_j^2 \\ \vdots \\ Q_j^{n_z-1} \end{pmatrix}, \qquad j = 0, 1, \ldots, n_r . \tag{3.14}$$

The radial boundary conditions (2.22), (2.23) are expressed by

$$\begin{aligned} P_{n_r} &= 0 , & Q_{n_r} &= 0 , \\ P_0 &= P_1 \delta_{m1} , & Q_0 &= Q_1 \delta_{m1} . \end{aligned} \tag{3.15}$$

Note that the condition at the origin for $m = 1$ is a first-order approximation of the true condition, but is expected to provide sufficient accuracy due to the use of a nonlinear mesh.

Representing partial derivatives in the $\eta\zeta$-plane with the standard second-order forms, the eigenvalue equations (2.19) take the form

$$\lambda P_j = U_j^{11} P_{j-1} + V_j^{11} P_j + W_j^{11} P_{j+1} + U_j^{12} Q_{j-1} + V_j^{12} Q_j + W_j^{12} Q_{j+1} , \qquad \lambda Q_j = U_j^{21} P_{j-1} + V_j^{21} P_j + W_j^{21} P_{j+1} + V_j^{22} Q_j , \tag{3.16}$$

$j = 1, 2, \ldots, n_r - 1$. Each coefficient matrix has the tridiagonal form

$$\{\alpha, \beta, \gamma\} \equiv \begin{pmatrix} \beta & \gamma & & & \\ \alpha & \beta & \gamma & & \\ & \ddots & \ddots & \ddots & \\ & & \alpha & \beta & \gamma \\ & & & \alpha & \beta \end{pmatrix} , \tag{3.17}$$

the uniform bands reflecting the fact that the eigenvalue equations possess no explicit dependence on z. If we introduce the notation

$$P = \begin{pmatrix} P_1 \\ P_2 \\ \vdots \\ P_{n_r-1} \end{pmatrix}, \qquad Q = \begin{pmatrix} Q_1 \\ Q_2 \\ \vdots \\ Q_{n_r-1} \end{pmatrix}, \qquad \xi = \begin{pmatrix} P \\ Q \end{pmatrix}, \tag{3.18}$$

the above system may be written in the symbolic form

$$F\xi = \lambda\xi , \tag{3.19}$$

where

$$F = \begin{pmatrix} F^{11} & F^{12} \\ F^{21} & F^{22} \end{pmatrix},$$

$$F^{JK} = \begin{pmatrix} V_1^{JK} + U_1^{JK}\delta_{m1} & W_1^{JK} & & & \\ U_2^{JK} & V_2^{JK} & W_2^{JK} & & \\ & \ddots & \ddots & \ddots & \\ & & U_{n_r-2}^{JK} & V_{n_r-2}^{JK} & W_{n_r-2}^{JK} \\ & & & U_{n_r-1}^{JK} & V_{n_r-1}^{JK} \end{pmatrix} , \qquad J, K = 1, 2 . \tag{3.20}$$

Note that although equation (3.19) is an eigenvalue equation, it is *not* to be thought of as the discrete analog of equation (2.13), since it assumes a different representation.

e) The Critical Length

The power method is inherently unsuited to the calculation of near-zero eigenvalues for the following reasons. First, close to marginal stability the dominant unstable eigenmodes tend to blend with marginally stable modes associated with disturbances of the distant field (see Fig. 8). Such modes are always present independent of the length of the flux tube. This difficulty is further compounded by the fact that near-zero eigenvalues require more accurate eigenfunctions to maintain comparable relative precision.

An obvious way to determine the eigenvalues of F is to solve $\det(F - \lambda I) = 0$, but this is expensive in terms of computer memory and time. Rather, we proceed as follows. We write the eigenvalue equations in the form

$$(F^{11} - \lambda I)P + F^{12}Q = 0 , \qquad F^{21}P + (F^{22} - \lambda I)Q = 0 . \tag{3.21}$$

It is possible to eliminate a variable from these equations. As shown in Appendix B, the matrix $F^{22} - \lambda I$ is nonsingular for all λ values of interest, so from the second of these equations

$$Q = -(F^{22} - \lambda I)^{-1} F^{21} P \,. \tag{3.22}$$

The tridiagonality of F^{22} means that, from a numerical viewpoint, $F^{22} - \lambda I$ is simple to invert. Substituting into the first of the above equations, we find

$$F_{1/2} P = 0 \,, \qquad F_{1/2}(\lambda, l) = (F^{11} - \lambda I) - F^{12}(F^{22} - \lambda I)^{-1} F^{21} \,, \tag{3.23}$$

and the condition for nontrivial eigenfunctions is det $F_{1/2}(\lambda, l) = 0$. Thus, λ as a function of l may be determined by specifying one of the parameters λ, l and varying the other until equation (3.23) is satisfied. Because of the nature of $\lambda_1(l)$ (see Fig. 5), it is best to specify l and then find the largest root of equation (3.23) when λ_1 is large, and to specify λ_1 and then find the smallest root of equation (3.23) when λ_1 is weakly positive.

We thus have a general method for the calculation of eigenvalues, and in particular near-critical eigenvalues for which the power method is unsuited since large accuracy in the eigenfunctions is required. A disadvantage of the method is that one must use root-finding methods to solve equation (3.23). However, it is placed at no disadvantage when calculating critical lengths, since the power method, and indeed all methods, must do likewise in this case.

IV. NUMERICAL RESULTS

a) Introduction

Our aim is to obtain converged eigenmodes of the helical kink for the class of fields with power-law twist, introduced in § II. There are two aspects to the problem of convergence: convergence of the iterative scheme for a given spatial mesh, and the requirement of obtaining results independent of the numerical representation. In § IV*b* the aspect of spatial resolution is investigated with reference to the well-studied problem of the critical length of the Gold-Hoyle field. In § IV*c* we calculate the dominant eigenvalues of the power-law family of equilibrium fields, and in § IV*d* the form of the dominant eigenfunctions is discussed. Finally, the nature of higher-*m* instabilities is discussed in § IV*e*.

b) Critical Length of the Gold-Hoyle Field

In all calculations to follow, it is important to know how distant the outer boundary must be placed so that any further increase has little physical effect. Also, for the sake of efficiency when performing calculations it is important to know the mesh nonlinearity which allows optimal representation of dominant unstable modes. In order to be able to determine such information and as a preliminary test of the methods, we check the critical length of the Gold-Hoyle field, first estimated by Hood and Priest (1981).

In Figure 2 the critical length $l_c(b)$ is graphed versus b. Figure 3 shows a "convergence graph" for a typical point on this curve. As can be seen, the true critical length for a given b is "sandwiched" between curves of $l_c(b, N, r_{1/2})$ versus $N = n_r = n_z$ for various

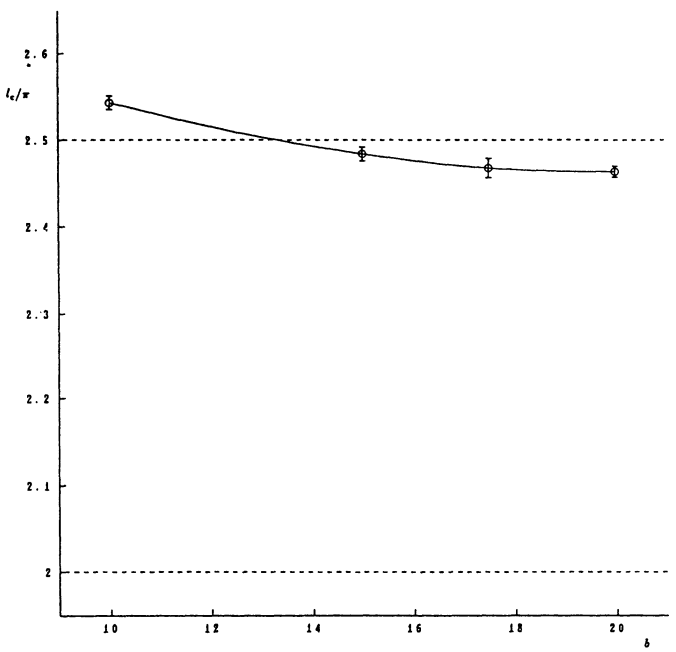

FIG. 2

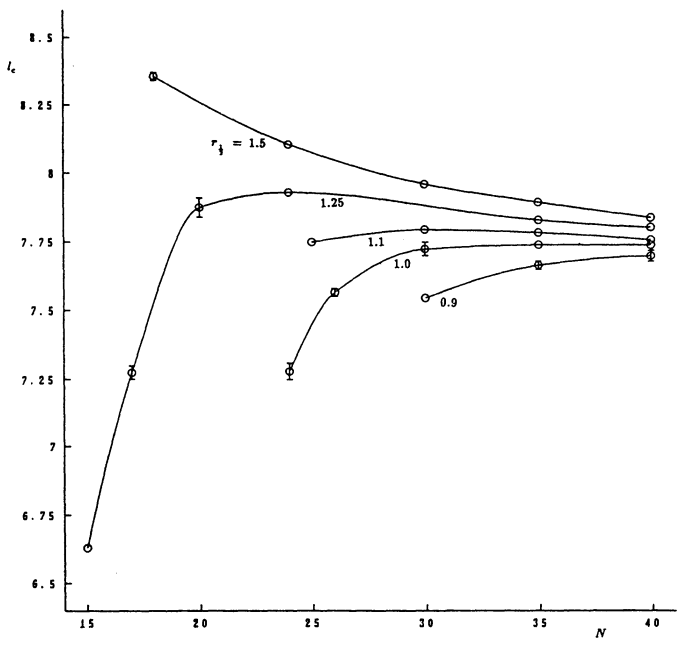

FIG. 3

FIG. 2.—Critical length l_c vs. b for the Gold-Hoyle field. Lower dashed line represents the sufficient bound for stability of Hood and Priest (1980); upper dashed line is the Hood and Priest (1981) estimate of the critical length.

FIG. 3.—"Convergence graph" for determining l_c for the Gold-Hoyle flux tube with $b = 20$, l_c is graphed vs. $N = n_r = n_z$ for various values of $r_{1/2}$. "Converged" value is taken as 7.74.

half-radii. Note that for each b there exists an optimal value of $r_{1/2}$ for which $l_c(b, N, r_{1/2})$ converges most rapidly with respect to N. The optimal half-radii are found to be of order unity, which is to be expected, since instabilities are driven in the "core region" $r \lesssim 1$.

The critical length decreases with b, as one would expect, since the inhibitive presence of an outer boundary tends to stabilize eigendisplacements. However, beyond $b \approx 15$, the critical length becomes insensitive to further increases in b. For an outer boundary of 20, it is found $l_c = 2.46\pi$, in good agreement with the estimate 2.5π calculated numerically by Hood and Priest (1981) and later checked by Einaudi and Van Hoven (1983), who approximated eigenmodes with a truncated Fourier series. That we obtain a lower value than Hood and Priest is of little surprise. In obtaining l_c, their spatial resolution is not maintained as b is varied since n_r is held constant on a uniform mesh, meaning that convergence with respect to b is bound to be false. Furthermore, there is no convincing display of convergence with respect to spatial resolution. In both cases, the effect will be to stabilize, leading to a critical length greater than the actual value.

c) *Force Eigenvalues of the Helical Kink*

We first demonstrate the influence of the outer boundary on the kink eigenvalue, for the case of the Gold-Hoyle field. The dominant eigenvalue λ_1 versus outer boundary for an unstable length of 10 is graphed in Figure 4. This illustrates, once again, the stabilizing nature of the outer boundary on an internal kink mode. Changes in b beyond $b \approx 15$ go roughly unnoticed by the fluid, but below this the instability weakens rapidly, becoming entirely suppressed for $b \lesssim 4$.

In the case of *stable* lengths, the eigenvalues are found to approach marginal stability from below as $b \to \infty$. This is because the dominant stable modes consist primarily of motion in the weak-field outer regions, generating feeble Lorentz forces which progressively weaken as $b \to \infty$.

The dependence of λ_1 upon tube length is shown in Figure 5 for $\nu = 0, \frac{1}{2}, 1$. We fix $b = 20$, $r_{1/2} = 1$, $n_r = 30$ and maintain z-resolution by fixing $n_z/l = 3$, that is a twist of roughly 19° between z points. This spatial mesh was shown to be adequate in the computation of the critical length and therefore should easily be sufficient for the calculation of eigenvalues outside the region of marginal stability. Since we have also employed extremely conservative criteria for terminating the power iterations we believe our eigenvalue estimates are generally accurate to within two or three significant figures: i.e., to within a typical relative error of a few percent. However, close to marginal stability ($\lambda < 10^{-3.5}$, say) precision becomes harder to maintain, and we would claim only qualitative accuracy of our results.

We note that each curve passes through zero at the critical length and increases with l, since the stabilizing influence of line-tying becomes less noticeable, "saturating" beyond $l \approx 20$ at a level of $O(10^{-2})$. The $\nu = 0$ curve approaches asymptotically the value $\lambda_1^{\max} = 1.769 \times 10^{-2}$, the maximum eigenvalue over all wavelengths for the infinite tube, as calculated by Sneyd and Craig (1989). The eigenvalues for long lengths are weaker than one would expect on dimensional grounds by two orders of magnitude. This means that nonlinear effects—whether stabilizing or destabilizing—will be more relatively significant. Dominant eigenvalues versus length for the Gold-Hoyle field were first calculated by Craig, McClymont, and Sneyd (1988), numerically, using a fully three-dimensional Cartesian framework. However, their results are underresolved with dominant eigenvalues almost an order of magni-

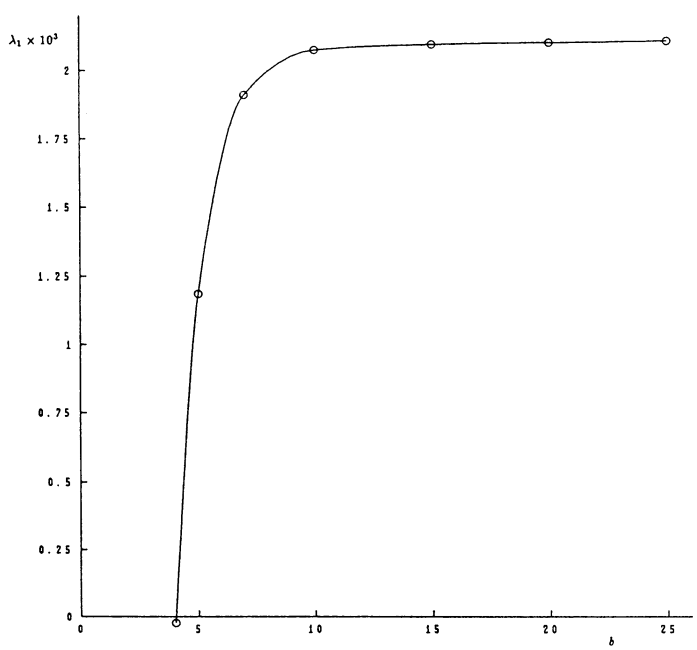

FIG. 4

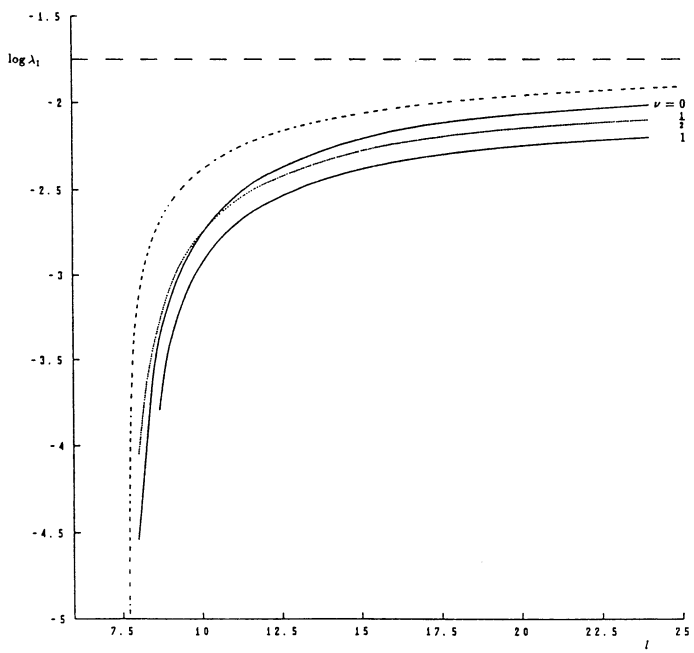

FIG. 5

FIG. 4.—Dominant eigenvalue λ_1 vs. b for an $l = 10$ Gold-Hoyle flux tube. The half-radius is 1, and $n_r = 40$, $n_z = 40$.

FIG. 5.—λ_1 vs. tube length for $\nu = 0, \frac{1}{2}$, and 1. Outer boundary is at 20, $r_{1/2} = 1$, $n_r = 30$, and z-resolution is maintained by fixing $n_z/l = 3$. Dashed curve represents eq. (4.1), the "heuristic curve" of Sneyd and Craig (1989).

tude smaller than those in Figure 5. Nonetheless, the same qualitative behavior is still observed, namely the tendency for longer flux tubes to be more unstable, with "saturation" beyond about four critical lengths.

Included in Figure 5 is the heuristic expression of Sneyd and Craig (1989), obtained upon assuming line-tying to raise the magnetic energy by M but to have an entirely local effect on modes:

$$\lambda_1 = \lambda_1^{\max}\left(1 - \frac{l_c}{l}\right), \qquad l_c = \frac{2M}{\lambda_1^{\max}}. \tag{4.1}$$

This approximate relation gives good qualitative agreement with the numerical curves. Interestingly enough, it also predicts "saturation" for a tube length ~ 4 times the critical length. Perhaps the most worthy feature of equation (4.1), however, is its universality. All loop configurations of the form (2.1) should have curves exhibiting this gross behavior. Furthermore, the relation should also be valid for all higher-m modes.

A salient feature of Figure 5 is that, for long lengths, the dominant eigenvalue can vary strongly with v. In particular, the long-length eigenvalues decrease by a factor of 2 in passing from $v = 0$ to $v = 1$. Preliminary results, to be published elsewhere, indicate that for $v \gtrsim 5$, the largest infinite-length eigenvalue is less than $O(10^{-3})$, at least one order of magnitude down on that of the Gold-Hoyle field. These results clearly demonstrate that the property of weak growth rates is a universal feature, and not just a peculiarity of the Gold-Hoyle field, a fact independently reinforced by the weak (order 10^{-2}) finite-length eigenvalues of the Lundquist field (Goedbloed and Hagebeuk 1972).

A further aspect of Figure 5 is the crossover of the $v = \frac{1}{2}$ and $v = 0$ curves, implying the $v = \frac{1}{2}$ curve has a lower critical length. This suggests that a given v curve crosses all other curves of lower v, and so the critical length decreases monotonically with v. Admittedly, the $v = \frac{1}{2}$ and $v = 1$ curves appear to contradict this statement, but this is almost certainly because the crossover occurs in a regime beyond our computational precision ($\lambda < 10^{-3.5}$). Our interpretation is reinforced by the fact that as $v \to \infty$, l_c approaches the limiting value 1.14π calculated semianalytically by Hood and Priest (1981). We emphasize that whereas maximal eigenvalues vary by more than two orders of magnitude in passing from $v = 0$ to $v = \infty$, the critical length varies by little more than a factor of 2. Thus, critical length calculations can be poor indicators of field stability characteristics. It is tempting to assume that a smaller critical length implies a more unstable field, but we have found a family of fields for which the opposite occurs.

The above results make good physical sense: as v increases, the field lines in the core region become less twisted, increasing the magnetic tension and so stabilizing kink displacements. However, if we increase v, then the length scale for variation in the magnetic field decreases, meaning that the effects of line-tying will only be noticed for smaller lengths.

d) The Form of the Eigenfunctions

We present eigenfunctions of the Gold-Hoyle field only, since for the moderate values of v considered, the eigenfunctions have little qualitative difference.

In Figure 6 we present graphs in $\eta\zeta$-space of the real and imaginary parts of $P = P_R + iP_I$ and $Q = Q_R + iQ_I$, for a Gold-Hoyle

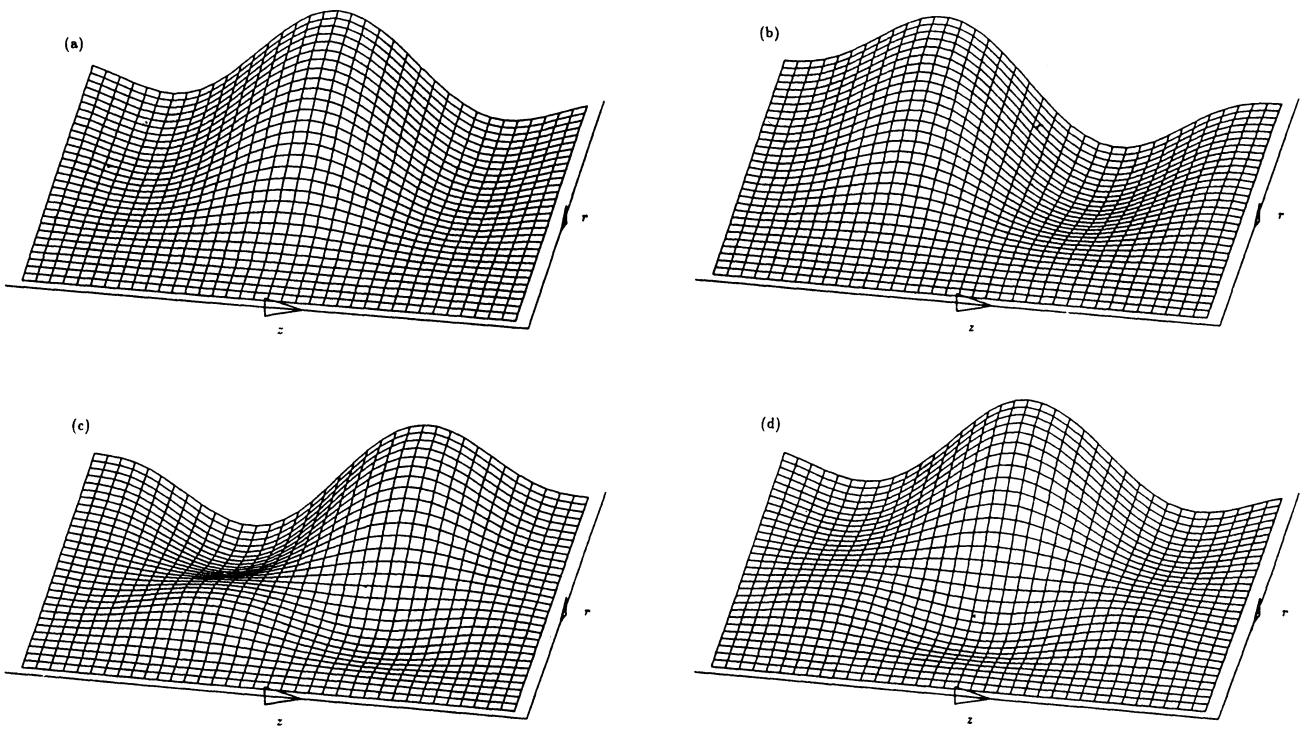

FIG. 6.—Graphs in $\eta\zeta$-space of (*a*) P_R, (*b*) P_I, (*c*) Q_R, and (*d*) Q_I for a Gold-Hoyle flux tube with $l = 12$. We have set $b = 20, r_{1/2} = 1, n_r = 30$, and $n_z = 36$. Vertical scale on the graphs remains arbitrary, and the arbitrary phase may be chosen so that the functions possess symmetry about $z = l/2$.

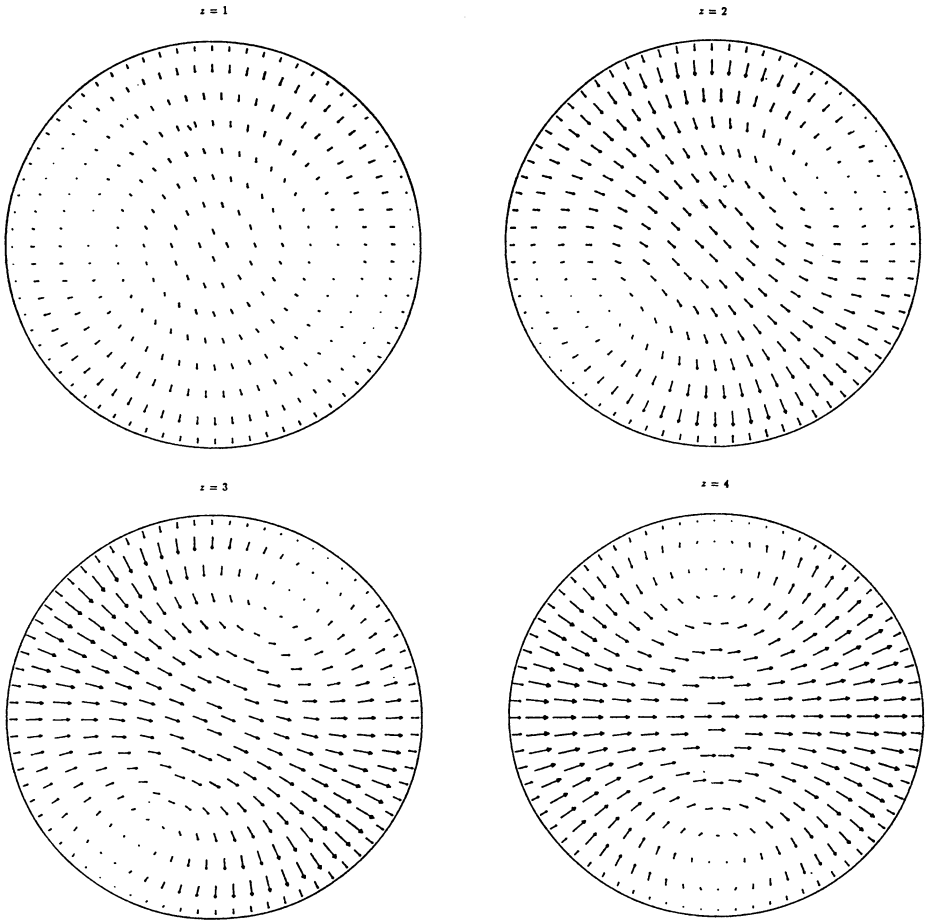

FIG. 7.—The projection of the displacement field onto the $\eta\theta$-planes situated at $z = 1, 2, 3, 4$ along a Gold-Hoyle flux tube with $l = 8$. Note the flow for $l/2 - z$ is a mirror image, along the $\theta = 0$ and π line, of that for z. We have set $b = 20, r_{1/2} = 1, n_r = 30$, and $n_z = 24$. Only selected r-points have been graphed, for purposes of clarity.

flux tube with an unstable length of 12. The eigenfunction is unique to within a real factor, which remains arbitrary, and a phase, which can be chosen so that P and Q have symmetry about $z = \frac{1}{2}l$.

Physical displacements are calculated from P and Q through the formula

$$\boldsymbol{\xi}(r, \theta, z) = \mathrm{Re}\ \{\boldsymbol{\xi}(r, z)e^{im\theta}\}\ , \tag{4.2}$$

where $\boldsymbol{\xi}(r, z)$ is given by equation (2.16). In Figure 7 we show the projection of $\boldsymbol{\xi}(r, \theta, z)$ onto various $\eta\theta$-planes along the z-axis, for a marginally unstable $l = 8$ Gold-Hoyle tube. The helical-kink nature of the instability, corkscrewing in the same sense as the field lines, is readily seen. The *onset* of a kink instability is demonstrated in Figure 8, where we show $\boldsymbol{\xi}(r, \theta, z)$ projected onto the $\eta\theta$-plane

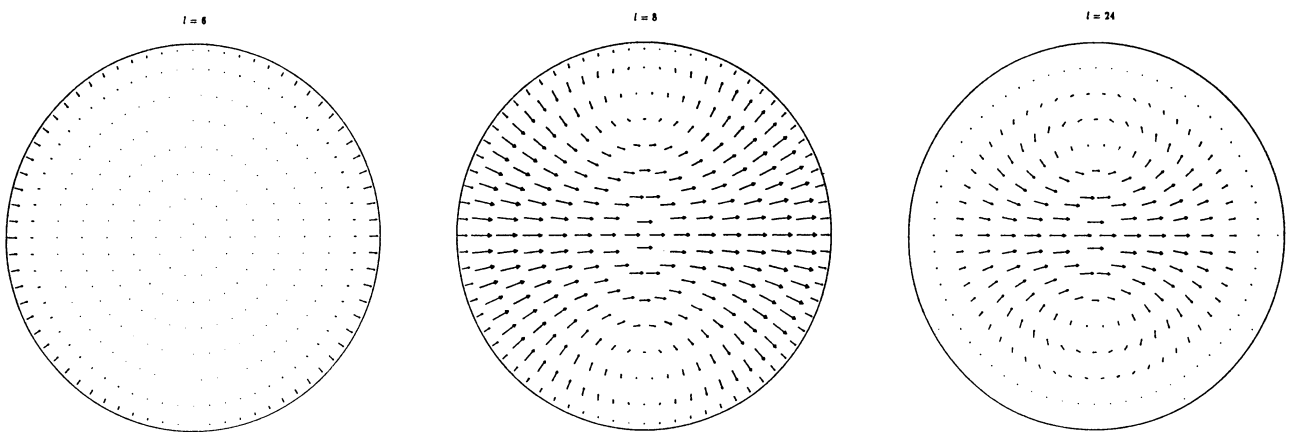

FIG. 8.—Projection of the displacement field onto the $\eta\theta$-plane midway along a Gold-Hoyle tube, showing the increased core penetration as l increases. We have taken $b = 20, r_{1/2} = 1, n_r = 30$, and $n_z/l = 3$. Only selected r-points have been graphed, for the purposes of clarity.

midway along the tube for $b = 20$ and $l = 6, 8, 24$. For the stable $l = 6$ tube, the dominant displacement is concentrated about the outer boundary, not penetrating into the inner region of higher magnetic tension. As $b \rightarrow \infty$, the oscillation frequency of such modes presumably tends to zero, since the field strength in the vicinity of the outer boundary becomes progressively weaker. For a marginally unstable length of 8 the displacement has penetrated into the core but remains relatively small, and as the length increases beyond this the instability becomes more confined to the core region.

The dependence of the axial oscillation upon tube length is illustrated in Figure 9, where we graph $P_R(0, z)$ and $P_I(0, z)$ for the Gold-Hoyle tube and representative lengths of 8, 16, 24. Note it is superfluous to present $Q(0, z)$, since it can be determined from $P(0, z)$ using equation (A5): $Q(0, z) = iP(0, z)$. For a near-critical length of 8, the disturbance is seen to be a "fundamental," and as the length increases, so the number of rotations of the helical kink progressively increases. Eventually, as $l \rightarrow \infty$, the dominant eigendisplacement $\xi(r, z) \rightarrow \xi(r)e^{ikz}$ for $k \approx -0.75$ (Sneyd and Craig 1989).

e) *Higher-m Instabilities*

Certain key results exist concerning the stability of higher-m modes in cylindrical flux tubes. The comparison theorems of Newcomb (1960) state that if the $m = 0$ and 1 modes of an infinite tube are stable, then so are all modes of higher m. The arguments

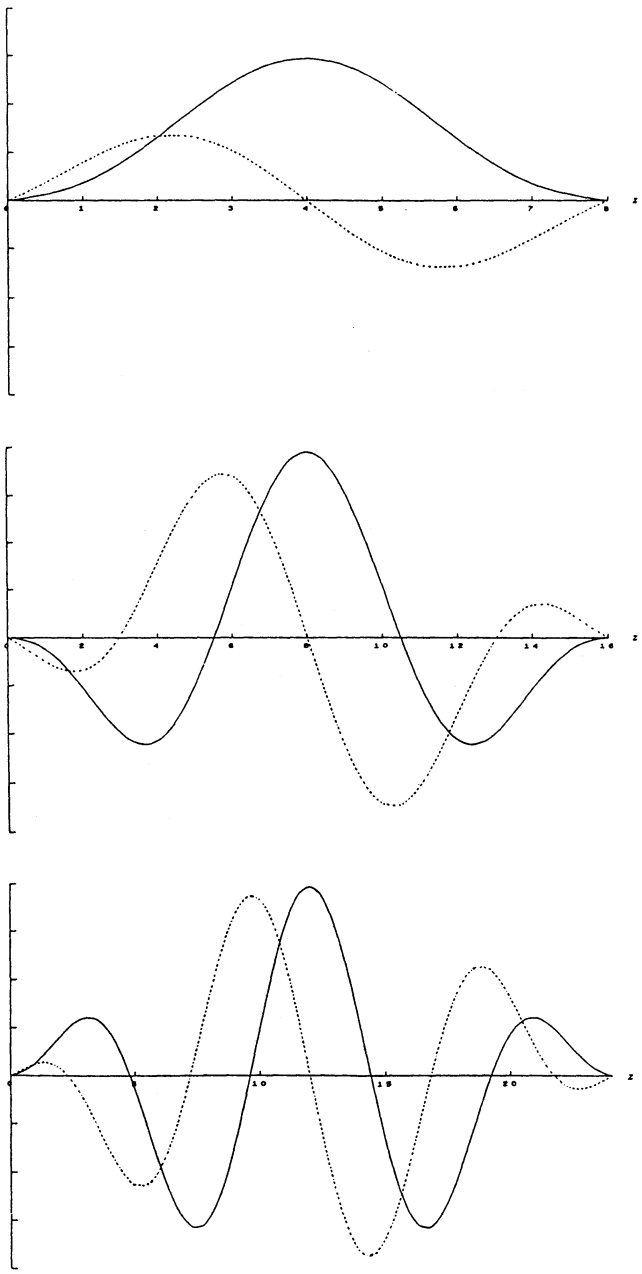

FIG. 9.—$P_R(0, z)$ (*solid*) and $P_I(0, z)$ (*dashed*) for Gold-Hoyle tubes of length $l = 8$, 16, and 24, demonstrating the increased number of kink rotations as l increases. We have taken $b = 20$, $r_{1/2} = 1$, $n_r = 30$, and $n_z/l = 3$.

of Einaudi and Van Hoven (1981) suggest that these comparison theorems also hold for the line-tied tubes considered here. It is of interest nonetheless to study higher-m modes, both to provide a computational check of this result and to quantify the magnitude of the instability. To date, most authors have considered only $m = 1$ modes (e.g., Raadu 1972), with the exception of Craig, McClymont, and Sneyd (1988), who analyze the linear stability of arbitrary force-free equilibria in Cartesian geometry, and so effectively modes of all m are present (see also Cargill, Hood, and Migliuolo 1986). In fact, Sneyd and Craig (1989) have shown that the $m = 1$ mode is dominant for infinite tubes with power-law twists, but the possibility remains that for moderate lengths some higher modes may dominate because their shorter wavelength could imply less sensitivity to line-tying.

As a first attack, we search for the critical length of the Gold-Hoyle $m = 2$ mode. This does exist, since for an infinite tube Sneyd and Craig (1989) find an $m = 2$ instability, only marginally weaker than $m = 1$. We adopt the values $n_r = 60$, a z-resolution of marginally greater than six points per unit length and $b = 20$, $l = 8$, $r_{1/2} = 1$, effectively doubling the resolution in anticipation of more oscillatory behavior. An instability was not found, however, which at least demonstrates that the $m = 2$ critical length exceeds that of $m = 1$; i.e., the decreased sensitivity to line-tying cannot overcome the effect of weakened instability in this case.

In summary, we have found no evidence thus far to upset the dominance of the $m = 1$ kink mode.

V. SIGNIFICANCE TO QUIESCENT AND FLARING CORONAL PLASMAS

A crucial requirement of any solar flare theory is its ability to convert stored energy into other forms in a time of 10^3 s or less. In fact, the failure to meet this requirement is the stumbling point of many flare mechanisms. Now it is often believed that the kink instability is the triggering mechanism for simple loop flares, and it is often stated that the instability has a time scale of order the Alfvén radial transit time (1–10 s), adequately small to explain rapid flaring. However, we have shown in § IV*b* that power-law twist profiles have growth times greater than this by an order of magnitude or more. Physically, we expect this to pertain to all monotonic increasing twist profiles. The existence of large growth times may not be surprising, since a kink mode with wavenumber k requires communication over length scales $2\pi a/k = O(10a)$, for the most unstable $k \approx m = 1$ modes, implying growth rates of order $0.1/t_A$. Furthermore, the scale times may still be sufficiently small to allow rapid flaring. More critically however, the power released by the kink mode has a dramatic cubic dependence on the growth rate. This means that the linear phase of the instability is at least three orders of magnitude less powerful than previously anticipated. Of course, since the linear forces are weak, nonlinear effects will be relatively more noticeable. These could serve either to accelerate or to suppress the instability.

Either way, our study of cylindrical flux tubes with power-law twist profiles is inconsistent with the notion of rapid collapse of coronal magnetic fields on the MHD time scale. Neither is it consistent with the longevity of quiescent coronal loops unless (i) finite pressure or toroidal effects are strongly stabilizing; (ii) nonlinear effects quash the instability; or (iii) individual loops are stabilized by the influence of neighboring flux tubes in the active region assemblage. This latter effect is quite possible, given the inherently feeble nature of the MHD instability.

VI. CONCLUSIONS

We have developed methods suited to determining the linear MHD stability of general cylindrically symmetric, line-tied force-free equilibria. We calculate the dominant eigenvalue versus tube length for the family of fields with twist proportional to r^v, indicating the universal behavior of a monotonic increase from zero, beyond the critical length, with "saturation" for lengths 3 or 4 times the critical length. The Gold-Hoyle field ($v = 0$) is the most unstable member of the family for long lengths, but is less resistant to the effects of line-tying and so possesses the highest critical length of the family.

However, our most important conclusion concerns the universality of small force eigenvalues for the dominant unstable mode, i.e., the corkscrew kink. We have found no evidence that higher-m modes dominate over $m = 1$, for the moderate lengths considered. The existence of surprisingly small growth rates impacts considerably on the power released in the linear phase: this is reduced by a factor of 1000 or more. Thus, our study effectively overrules the rapid MHD collapse of twisted flux tubes as a means of triggering the initial phase of the solar flare. Our results are more consistent with a very slow quasi-steady movement away from equilibrium—a movement that involves an almost negligible release of magnetic energy.

The authors acknowledge the interest shown, and helpful comments given, by staff of the Mathematics Department of the University of Waikato during the course of research. Calculations were performed on Microvax II computers, purchased by a university grants committee research grant.

APPENDIX A

To derive the boundary conditions on the axis, we first demand finiteness as $r \to 0$ of the (dimensionless) current density $\boldsymbol{j} = \nabla \times \boldsymbol{B}$. This, in turn, requires upon inspection of equation (2.18) that the twist $T = B_\theta/rB_z$ be finite as $r \to 0$. The Lorentz force $\boldsymbol{F}(\xi)$ must be finite at $r = 0$, so from the eigenvalue equations (2.19) we must have

$$\frac{P_r}{r} - \frac{P}{r^2} + im\left(\frac{Qr}{r} - \frac{Q}{r^2}\right), \qquad -\frac{mQ}{r^2} + i\left(\frac{P_r}{r} + \frac{P}{r^2}\right), \tag{A1}$$

finite as $r \to 0$. It follows by application of *l'*Hôpital's rule that

$$P_r(0, z) + imQ_r(0, z) = 0, \qquad 3P_r(0, z) + imQ_r(0, z) = 0. \tag{A2}$$

Thus, the conditions on the derivatives of P and Q are

$$\begin{aligned} &P_r(0, z) = 0\,, \quad Q_r(0, z) = 0\,, \quad &&\text{if } m \neq 0\,; \\ &P_r(0, z) = 0\,, &&\text{if } m = 0\,. \end{aligned} \tag{A3}$$

We must also have $\nabla\xi$ finite at $r = 0$, from which it follows that

$$imP(0, z) - Q(0, z) = 0\,, \quad imQ(0, z) + P(0, z) = 0\,. \tag{A4}$$

Thus,

$$\begin{aligned} &iP(0, z) = Q(0, z) = 0\,, \quad &&\text{if } m \neq 1\,; \\ &iP(0, z) = Q(0, z)\,, &&\text{if } m = 1\,. \end{aligned} \tag{A5}$$

The first of equations (A5) and the first of (A3) for the case $m = 1$ provide the boundary conditions stated in equation (2.23). These conditions are not unique; for example, we could equally well choose the set $P(0, z) = Q(0, z) = 0$ for $m = 0$ and $P_r(0, z) = Q_r(0, z) = 0$ for $m \neq 0$, which incidentally indicates the kink nature of all $m \neq 0$ instabilities. However, from a numerical viewpoint, it is obviously less desirable to adopt this latter set, since derivative conditions are usually more difficult to implement.

As already mentioned, Hood and Priest (1981) derive these same conditions by expanding all quantities in a power series for small r, restricting $\boldsymbol{B}$ to the form:

$$B_z = 1 + b_2 r^2 + b_4 r^4 + \cdots\,, \quad B_\theta = b_1 r + b_3 r^3 + b_5 r^5 + \cdots\,. \tag{A6}$$

This is by no means the most general form of the field: for instance, suppose T^2 has the expansion

$$T^2 = \sum_{n=0}^{\infty} t_n r^{na}\,, \tag{A7}$$

for a real. Substituting into equation (2.4), it is found that

$$\begin{aligned} B_z &= 1 + r^2 \sum_{n=0}^{\infty} c_n^{(2)} r^{na} + r^4 \sum_{n=0}^{\infty} c_n^{(4)} r^{na} + \cdots\,, \\ B_\theta &= rT^2 + r^3 \sum_{n=0}^{\infty} r^{na} \sum_{k=0}^{n} c_k^{(2)} t_{n-k} + r^5 \sum_{n=0}^{\infty} r^{na} \sum_{k=0}^{n} c_k^{(4)} t_{n-k} + \cdots\,, \end{aligned} \tag{A8}$$

where

$$c_n^{(2)} = t_n\left(\frac{1}{2}\frac{na}{na+2} - 1\right), \quad c_0^{(4)} = t_0^2\,, \quad c_1^{(4)} = t_0 t_1\left[2 - \frac{a(a+3)}{(a+2)(a+4)}\right], \ldots\,.$$

In general, we need only demand T finite and smooth as $r \to 0$, as mentioned above.

APPENDIX B

We wish to determine sufficient conditions for the nonsingularity of $F^{22} - \lambda I$. Note first that

$$\det\,(F^{22} - \lambda I) = \prod_{j=1}^{n_r - 1} \det\,(V_j^{22} - \lambda I)\,, \tag{B1}$$

so $F^{22} - \lambda I$ is nonsingular if and only if the individual blocks $V_j^{22} - \lambda I$ for $j = 1, 2, \ldots, n_r - 1$ are nonsingular. It is easily shown that the tridiagonal matrices V_j^{22} have the explicit form

$$V_j^{22} = \{\alpha_j, \beta_j, \gamma_j\}\,, \quad \alpha_j = \gamma_j = \frac{e_z^2}{\Delta^2}\,, \quad \beta_j = -\frac{m^2}{r_j^2} - 2\frac{e_z^2}{\Delta^2}\,, \tag{B2}$$

(see eq. [3.17]). A general tridiagonal matrix $\{\alpha, \beta, \gamma\}$ with $\alpha, \gamma \neq 0$ is nonsingular if $|\beta| \geq |\alpha| + |\gamma|$ (Isaacson and Keller 1966). Thus, $F^{22} - \lambda I$ is invertible if

$$\lambda + \frac{m^2}{r_j^2} \geq 0\,, \quad j = 1, 2, \ldots, n_r - 1\,, \tag{B3}$$

which is certainly satisfied for λ positive or zero, the case of physical interest.

REFERENCES

Anzer, U. 1968, *Solar Phys.*, **3**, 298.
Bernstein, I. B., Frieman, E. A., Kruskal, M. D., and Kulsrud, R. M. 1958, *Proc. Roy. Soc. London, A*, **244**, 17.
Cargill, P. J., Hood, A. W., and Migliuolo, S. 1986, *Ap. J.*, **309**, 402.
Craig, I. J. D., McClymont, A. N., and Sneyd, A. D. 1988, *Ap. J.*, **335**, 441.
Craig, I. J. D., and Sneyd, A. D. 1986, *Ap. J.*, **311**, 451.
———. 1989, *Comput. Math. Appl.*, **17**, 1149.
Einaudi, G., and Van Hoven, G. 1981, *Phys. Fluids*, **24**, 1092.
———. 1983, *Solar Phys.*, **88**, 163.
Goedbloed, J. P., and Hagebeuk, H. J. L. 1972, *Phys. Fluids*, **15**, 1090.

Hood, A. W., and Priest, E. R. 1979, *Solar Phys.*, **64**, 303.
———. 1980, *Solar Phys.*, **66**, 113.
———. *Geophys. Ap. Fluid Dyn.*, **17**, 297.
Isaacson, E., and Keller, H. 1966, *Analysis of Numerical Methods* (New York: Wiley).
Kruskal, M., and Tuck, J. L. 1958, *Proc. Roy. Soc. London, A*, **245**, 222.
Lanczos, C. 1956, *Applied Analysis* (New York: Prentice-Hall).
Newcomb, W. A. 1960, *Ann. Phys.*, **10**, 232.
Raadu, M. 1972, *Solar Phys.*, **22**, 425.
Sneyd, A. D., and Craig, I. J. D. 1989, *Ap. Space. Sci.*, **151**, 265.
Švestka, Z. 1976, *Solar Flares* (Dordrecht: Reidel).
Van Hoven, G. 1981, in *Solar Flare Magnetohydrodynamics*, ed. E. R. Priest (New York: Gordon & Breach), p. 217.
Wilkinson, J. H. 1965, *The Algebraic Eigenvalue Problem* (Oxford: Oxford University Press).

I. J. D. Craig and B. J. Foote: Department of Mathematics, University of Waikato, Hamilton, New Zealand